Teck Chew Ng
Singapore Institute of Manufacturing Technology
71 Nanyang Drive, Singapore
tcng@SIMTech.a-star.edu.sg

Martin Adams
School of Electrical & Electronics Engineering
Nanyang Technological University, Singapore
eadams@ntu.edu.sg

Javier Ibañez-Guzmán
Renault – Research Division – Electronics Systems
Department, France
javier.ibanez-guzman@renault.com

Bayesian Estimation of Follower and Leader Vehicle Poses with a Virtual Trailer Link Model

PROOF ONLY

Abstract

Autonomous Vehicle Following can be achieved if the poses of both the follower and leader vehicles are continuously estimated. This can be achieved by using a Bayesian estimation technique together with a virtual trailer link model. The advantage of such a model is that the follower vehicle will trail a virtual trailer, modeled as an attachment to the leader vehicle, instead of the leader vehicle itself, so that a safe spacing between the two vehicles is guaranteed. The key to a tractable solution to this vehicle following problem is the justifiable assumption that the pose of the follower vehicle is statistically independent of that of the leader. This assumption is valid when conditioned on the history of the follower vehicle's inputs and the sensor observations made by the follower vehicle. Hence, a factored solution to the joint estimate of the follower and leader poses can be formulated. Due to the factored solution, the pose of the follower vehicle is estimated separately using a recursive estimator. In a separate estimator, the poses of the virtual tailer and the leader vehicle are augmented in the tracking process of the leader vehicle. The aim is to command the follower vehicle to trail the estimated pose of the virtual trailer link model. The pose of the virtual trailer is computed with an on-board sensor mounted on the follower vehicle. A case study on the implementation of the proposed formulation, using an Extended Kalman Filter as the main estimator, is presented. First, simulation results are presented. To make the simulation results comparable to the actual system, the variances of sensor measurements are set according to real sensor data-sheet values. Various types of vehicle maneuver, such as straight paths and clothoids with left and right transition paths, are considered. Real experiments are also carried out in a car park. A comparison of the estimated paths and the best available ground truth is presented. The path deviations of the proposed system are also compared with similar systems in the literature.

KEY WORDS—vehicle following, target tracking, virtual trailer

1. Introduction

A well-designed vehicle following system can significantly impact the traffic flow on highways and in the city. On highways, commercially-available vehicle following systems, such as Automatic Cruise Control (ACC) systems, have been widely used for keeping a safe distance between vehicles and improving traffic flowrate. On the other hand, in the city area, traffic is characterized by low speed, traffic jams and tight curves. As ACC systems can only be useful in high speed traffic, typically more than $50\,\mathrm{km\,h^{-1}}$, they are not suitable for operations in the city area. Hence, there is a need to extend the ACC concept to more complex situations such as dense traffic in city areas.

Research in vehicle following has attracted the attention of several researchers in the past decades, particularly in the USA and Europe where safety, energy consumption and traffic congestion are the primary motivator (Sheikholeslam and Desoer 1991; Committee on Army UGV Technology 2002). Major contributions are from the Chauffeur Project (Europe), the PATH program (USA), the Intelligent Transportation System program in Japan and the CyberCar project in France

The International Journal of Robotics Research
Vol. 00, No. 00, Xxxxxxxx 2007, pp. 000–000
DOI: 10.1177/0278364907084262
©SAGE Publications 2007 Los Angeles, London, New Delhi and Singapore
Figures 1–2, 4–12, 14–16, 18–20 appear in color online: http://ijr.sagepub.com

(INRIA) (National Academy of Engineering 1998; Parent 2004). The majority of the systems developed use either inter-vehicle communication systems (Swaroop and Yoon 1999; Borodani 2000) or wayside infrastructure (e.g. embedded road markers on road networks) to vehicle communication systems (Fujioka and Suzuki 1994) to achieve vehicle following. Other systems use a path planner together with an inter-vehicle communication system (Chen et al. 2004; Ng et al. 2004).

These systems have various disadvantages. For example, the use of information from the leader vehicle transmitted to the led vehicle may not be available in certain conditions. This also requires additional costs and confines the use of the system to a certain type of leader vehicle.

There have been few endeavors on modeling an entire vehicle following system. From the literature, most research efforts in this domain focus on the controllers of the follower vehicle. Two common controllers, longitudinal and lateral, have been implemented to guarantee that a follower vehicle trails a leader, but little attention was paid to following the actual trajectory of the leader vehicle. The longitudinal controller maintains a set distance between the two vehicles, and the lateral controller minimizes the alignment angles between them. The combination of both controllers achieves a 'towing' effect (Borodani 2000).

Work which is similar to the system proposed here has been suggested by Lu and Tomizuka (2005), Wang and Xu (2000) and Stefan (2000). Lu and Tomizuka (2005) used the information from an on-board laser scanner, which measured the relative position of the leader vehicle with respect to the follower vehicle for vehicle following. The position of the follower vehicle was obtained from magnetic markers embedded in the road and a filter was implemented to recursively estimate the position of the leader vehicle.

Wang and Xu (2000) implemented a vehicle following system by imitating human driving practices. A virtual point was estimated based on the position of the leader vehicle. The follower vehicle was then commanded to trail this virtual point so as to achieve vehicle following.

Stefan (2000) proposed a path-based vehicle following system. The pose of the follower vehicle was estimated from the extracted road features. The position of the leader vehicle was estimated using a camera. All of the above systems did not provide a mathematical formulation of the vehicle following system as a whole. Furthermore, only the position of the leader vehicle is estimated. The orientation of the leader vehicle, which is important for vehicle following, was omitted.

The research work in this paper is motivated by the above issues. A probabilistic method for vehicle following systems is proposed. Theoretically, the proposed system in this work can be operated at high speed. However, due to the unavailability of a high speed road vehicle, the maximum speed of the proposed system will be limited to $10\,\mathrm{km\,h^{-1}}$, which is the maximum allowable speed of our experimental RobuCar vehicle. To maintain a safe inter-vehicle distance and at the same time minimize the path deviation in the vehicle following system, we propose a *virtual trailer* (VT) Link model. The concept of the VT link model was first introduced in our earlier work (Ng et al. 2005). In this model, the vehicle following system is formulated as if the leader vehicle is pulling a trailer. It was shown that a VT containing at least two links of equal length is necessary for a follower vehicle to be able to exactly execute the identical trajectory of the leader vehicle. This is based on the assumption that the majority of roads are a combination of straight and circular paths. It was also shown that a two-link trailer is a sensible choice, since increasing the number of links would reduce the string stability of the platoon (Swaroop and Hedrick 1996). With this VT link model, we can command the follower vehicle to safely follow the trajectory of the virtual trailer link and this, in effect, follows the trajectory of the leader vehicle.

There are several advantages in implementing the VT model for vehicle following.

- There is no need for inter-vehicle or wayside vehicle communication. This implies that our follower vehicle can switch to tracking and following any vehicle on the road without adjustment.
- By performing path following rather than pure pursuit of the leader vehicle, we can prevent the follower vehicle from cutting corners (hitting the curbs and other obstacles) which are beyond the field of view of the sensor. This is particularly important when the leader vehicle is making a sharp turn.

Due to the stochastic nature of the system and measurement models, a Bayesian formulation is used to represent the state of the system. The probability density functions (pdfs) of the states of the leader and follower vehicles are sought as a solution to the estimation problem. When conditioned on the history of the follower's inputs and sensor observations, a factored solution, which assumes that the poses of the follower and leader vehicles are statistically independent, is reasonable (Thrun et al. 2005). The vehicle following system is partitioned as two separate estimation processes: one for the localization of the follower and the other to track the leader vehicle and the pose of the virtual trailer link.

Tests under simulated and real environmental conditions have demonstrated that the proposed Bayesian formulation of the vehicle following system with the VT link model is viable for implementation. Furthermore, the performance of our vehicle following system is compared with the systems developed by Stefan (2000), Wang and Xu (2000) and Lu and Tomizuka (2005). Results show that our system can perform at least two times better in terms of path deviations between the leader and follower vehicles than the above published results.

PROOF ONLY

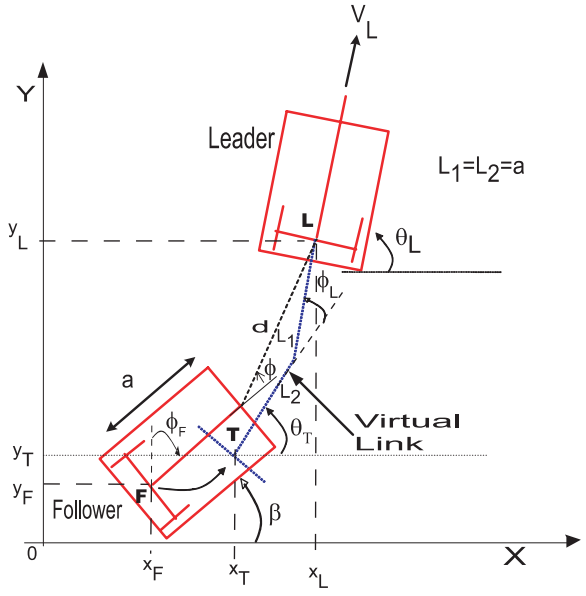

Fig. 1. At any time instant, the follower perceives the pose of the leader with an on-board sensor. The pose **T** of the virtual trailer link is then computed. The follower will be commanded to move to the new position **T**. The whole process will be repeated at the next time instant.

2. Virtual Trailer Link Model for the Vehicle Following System

As our earlier work (Ng et al. 2005) has already provided an analysis of the feasibility of the virtual trailer link model, it will only be summarized here. Figure 1 shows a typical configuration of the leader and follower vehicles. At any time k, the follower vehicle uses an on-board sensor to compute the pose of the leader vehicle $\mathbf{L} = [x_L \;\; y_L]^T$ with respect to a given global frame. This is derived as:

$$\begin{bmatrix} x_L \\ y_L \end{bmatrix} = \begin{bmatrix} x_F \\ y_F \end{bmatrix} + \begin{bmatrix} \cos\beta & -\sin\beta \\ \sin\beta & \cos\beta \end{bmatrix} \times \begin{bmatrix} a + d\cos\phi \\ d\sin\phi \end{bmatrix} \quad (1)$$

where a is the distance between the front and the rear wheels of the follower vehicle and d is the distance between the center of the rear axle of the leader vehicle to the sensor mounting position on the follower vehicle. ϕ is the bearing of the leader vehicle as perceived by the sensor; ϕ_F is the orientation of the follower vehicle with respect to a known reference frame and $\beta = \pi/2 - \phi_F$.

The position of the virtual trailer (**T** in Figure 1) at time k is :

$$\mathbf{T} = \begin{bmatrix} x_T \\ y_T \end{bmatrix} = \mathbf{L} - L_1 \begin{bmatrix} \cos\theta_L \\ \sin\theta_L \end{bmatrix} - L_2 \begin{bmatrix} \cos\theta_T \\ \sin\theta_T \end{bmatrix} \quad (2)$$

where L_1 and L_2 are the lengths of the virtual trailer links. As shown in Ng et al. (2005), the path deviation between the leader vehicle and the virtual trailer can be minimized if $L_1 = L_2 = a$. θ_L and θ_T are the orientations of the leader vehicle and the corresponding virtual trailer, respectively (Figure 1).

The follower is then commanded to move to the virtual point **T**. At the next time, $k+1$, the follower will re-acquire the new pose of the leader, subject to the availability of the sensor data, and the whole process is repeated iteratively.

3. Problem Formulation

For vehicle following systems, the poses of the follower and leader vehicles with respect to a known reference frame, or the relative poses of the vehicles, are needed. Mathematically, the complete vehicle following system can be formulated as a probability density function (pdf)[1]:

$$P(\mathbf{x}_{F,k}, \mathbf{x}_{L,k} | \mathbf{U}_k, \mathbf{Z}_k) \quad (3)$$

where $\mathbf{x}_{F,k}$ and $\mathbf{x}_{L,k}$ are the poses of the follower and leader vehicles respectively at time k, $\mathbf{U}_k = (u_0, u_1, ..., u_k)$ is the history of the control inputs (for example, the speed and steering angle commands) of the follower vehicle and $\mathbf{Z}_k = (\mathbf{z}_0, \mathbf{z}_1, ..., \mathbf{z}_k)$ is the history of sensor measurement data collected up to and including time instant k. For a tractable solution to the vehicle following problem, the following usual assumptions are made.

- The vehicle following function is a Markov process and the current measurement $\mathbf{z}_k$ is independent of $\mathbf{Z}_{k-1}$ and $\mathbf{U}_k$, when conditioned on the pose of the follower vehicle. Hence,

$$P(\mathbf{x}_{F,k}, \mathbf{x}_{L,k} | \mathbf{U}_k, \mathbf{Z}_k) \propto P(\mathbf{z}_k | \mathbf{x}_{F,k}, \mathbf{x}_{L,k}) P(\mathbf{x}_{F,k}, \mathbf{x}_{L,k} | \mathbf{U}_k, \mathbf{Z}_{k-1}). \quad (4)$$

- Two separate sensors may be used in the pose estimation process. For example, odometry may be used for the localization of the follower vehicle while a range sensor may be used to acquire the pose of the leader vehicle. Hence, the measurement vector $\mathbf{Z}_k$ may be expressed

1. The lowercase notation, e.g. $\mathbf{x}_k$ denotes the current state and the uppercase notation, e.g. $\mathbf{X}_k$ denotes the entire history of the state up to and including time k.

PROOF ONLY

as two independent measurement vectors, when conditioned on the pose of the follower:

$$\mathbf{Z}_k = (\mathbf{z}_0^{\mathrm{p}}, \mathbf{z}_0^{\mathrm{r}}, \mathbf{z}_1^{\mathrm{p}}, \mathbf{z}_1^{\mathrm{r}}, ..., \mathbf{z}_k^{\mathrm{p}}, \mathbf{z}_k^{\mathrm{r}}) = (\mathbf{Z}_k^{\mathrm{p}}, \mathbf{Z}_k^{\mathrm{r}}) \quad (5)$$

where $\mathbf{Z}_k^{\mathrm{p}} = (\mathbf{z}_0^{\mathrm{p}}, \mathbf{z}_1^{\mathrm{p}}, ..., \mathbf{z}_k^{\mathrm{p}})$ and $\mathbf{Z}_k^{\mathrm{r}} = (\mathbf{z}_0^{\mathrm{r}}, \mathbf{z}_1^{\mathrm{r}}, ..., \mathbf{z}_k^{\mathrm{r}})$ are the proprioceptive sensor measurement vector and range sensor measurement vector respectively, obtained up to, and including, time k. Hence,

$$\begin{aligned} & P(\mathbf{z}_k|\mathbf{x}_{\mathrm{F},k}, \mathbf{x}_{\mathrm{L},k}) P(\mathbf{x}_{\mathrm{F},k}, \mathbf{x}_{\mathrm{L},k}|\mathbf{U}_k, \mathbf{Z}_{k-1}) \\ = \; & P(\mathbf{z}_k^{\mathrm{p}}, \mathbf{z}_k^{\mathrm{r}}|\mathbf{x}_{\mathrm{F},k}, \mathbf{x}_{\mathrm{L},k}) \\ \times \; & P(\mathbf{x}_{\mathrm{F},k}, \mathbf{x}_{\mathrm{L},k}|\mathbf{U}_k, \mathbf{Z}_{k-1}^{\mathrm{p}}, \mathbf{Z}_{k-1}^{\mathrm{r}}) \\ = \; & P(\mathbf{z}_k^{\mathrm{p}}|\mathbf{x}_{\mathrm{F},k}, \mathbf{x}_{\mathrm{L},k}) P(\mathbf{z}_k^{\mathrm{r}}|\mathbf{x}_{\mathrm{F},k}, \mathbf{x}_{\mathrm{L},k}) \\ \times \; & P(\mathbf{x}_{\mathrm{F},k}, \mathbf{x}_{\mathrm{L},k}|\mathbf{U}_k, \mathbf{Z}_{k-1}^{\mathrm{p}}, \mathbf{Z}_{k-1}^{\mathrm{r}}). \end{aligned} \quad (6)$$

- As the sensor measurement, $\mathbf{z}_k^{\mathrm{p}}$ will be used for the estimation of the pose of the follower vehicle, it will not be affected by the pose of the leader vehicle. Then $\mathbf{z}_k^{\mathrm{p}}$ can be assumed to be independent of $\mathbf{x}_{\mathrm{L},k}$, when conditioned on the current state of the follower vehicle. Hence,

$$P(\mathbf{z}_k^{\mathrm{p}}|\mathbf{x}_{\mathrm{F},k}, \mathbf{x}_{\mathrm{L},k}) = P(\mathbf{z}_k^{\mathrm{p}}|\mathbf{x}_{\mathrm{F},k}). \quad (7)$$

- In the vehicle following function, a control command (e.g. steering angle and velocity) to be issued to the follower vehicle has to be computed based on the pose of the leader vehicle. This will affect the future pose of the follower vehicle. Thus, the state of the follower vehicle is statistically independent of the state of the leader when conditioned on the history of the inputs to, and observations made from, the follower vehicle. Hence,

$$\begin{aligned} & P(\mathbf{x}_{\mathrm{F},k}, \mathbf{x}_{\mathrm{L},k}|\mathbf{U}_k, \mathbf{Z}_{k-1}^{\mathrm{p}}, \mathbf{Z}_{k-1}^{\mathrm{r}}) \\ = \; & P(\mathbf{x}_{\mathrm{F},k}|\mathbf{U}_k, \mathbf{Z}_{k-1}^{\mathrm{p}}, \mathbf{Z}_{k-1}^{\mathrm{r}}) P(\mathbf{x}_{\mathrm{L},k}|\mathbf{U}_k, \mathbf{Z}_{k-1}^{\mathrm{r}}). \end{aligned} \quad (8)$$

- The history of the sensor measurement, $\mathbf{Z}^{\mathrm{r}}$, will be used for the estimation of the pose of the leader vehicle. Hence, the pose of the follower vehicle will not be affected by it, when conditioned on the history of the inputs to the follower, and the observations $\mathbf{Z}^{\mathrm{p}}$ made:

$$P(\mathbf{x}_{\mathrm{F},k}|\mathbf{U}_k, \mathbf{Z}_{k-1}^{\mathrm{p}}, \mathbf{Z}_{k-1}^{\mathrm{r}}) = P(\mathbf{x}_{\mathrm{F},k}|\mathbf{U}_k, \mathbf{Z}_{k-1}^{\mathrm{p}}). \quad (9)$$

- The pose of the leader vehicle $x_{\mathrm{L},k}$ is independent of the history of the inputs to the follower conditioned on the history of the observations (of the leader):

$$P(\mathbf{x}_{\mathrm{L},k}|\mathbf{U}_k, \mathbf{Z}_{k-1}^{\mathrm{r}}) = P(\mathbf{x}_{\mathrm{L},k}|\mathbf{Z}_{k-1}^{\mathrm{r}}). \quad (10)$$

By consolidating equations (3)–(10), the formulation for the vehicle following model can be factored as:

$$\begin{aligned} & P(\mathbf{x}_{\mathrm{F},k}, \mathbf{x}_{\mathrm{L},k}|\mathbf{U}_k, \mathbf{Z}_k) \\ \propto \; & \underbrace{P(\mathbf{z}_k^{\mathrm{p}}|\mathbf{x}_{\mathrm{F},k}) P(\mathbf{x}_{\mathrm{F},k}|\mathbf{U}_k, \mathbf{Z}_{k-1}^{\mathrm{p}})}_{\text{Localization of follower}} \\ \times \; & \underbrace{P(\mathbf{z}_k^{\mathrm{r}}|\mathbf{x}_{\mathrm{F},k}, \mathbf{x}_{\mathrm{L},k}) P(\mathbf{x}_{\mathrm{L},k}|\mathbf{Z}_{k-1}^{\mathrm{r}})}_{\text{Tracking of leader vehicle w.r.t follower}}. \end{aligned} \quad (11)$$

Thus, we can conclude that the joint posterior for the vehicle following system can be factored into two separate estimation processes, one for the localization of the follower while the other is used to track the leader vehicle.

4. System Architecture

A simplified block diagram of the vehicle following system consists of two feedback loops as shown in Figure 2. The inner loop comprises a motion controller that maintains the stable traction of the vehicle. The outer loop guides the vehicle to follow the estimated trajectory of the leader vehicle. The follower vehicle is assumed to have on-board sensors, which have the capability of estimating the orientation of the leader vehicle with respect to the follower vehicle's frame of reference. The process of implementing the vehicle following system can be sub-divided into the following three critical components:

- localization of the follower vehicle;
- detection and tracking of the target vehicle; and
- following the leader vehicle.

The first two components are individually addressed. The third component involves the control of the follower and will not be discussed in this paper.

In the subsequent sections, we will be using the Extended Kalman Filter (EKF) extensively, the derivation and notation for which can be found in Bar-Shalom and Li (2001).

5. Implementation

5.1. Localization of the Follower Vehicle

The reference coordinate system and the pose of the follower vehicle are shown in Figure 3. The Ackerman model (Dissanayake et al. 2001) is used to describe the motion of this vehicle.

A simple method for localization is via dead reckoning sensors such as wheel encoders. Unfortunately, dead-reckoning involves direct instrument integration, causing unbounded errors to be accumulated over time.

PROOF ONLY

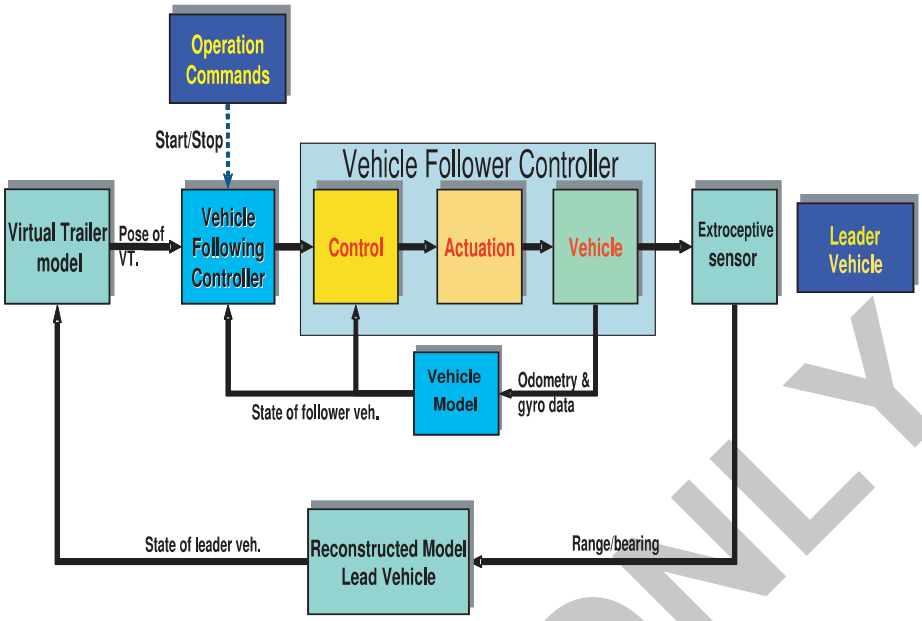

Fig. 2. Control block diagram for the proposed vehicle following system.

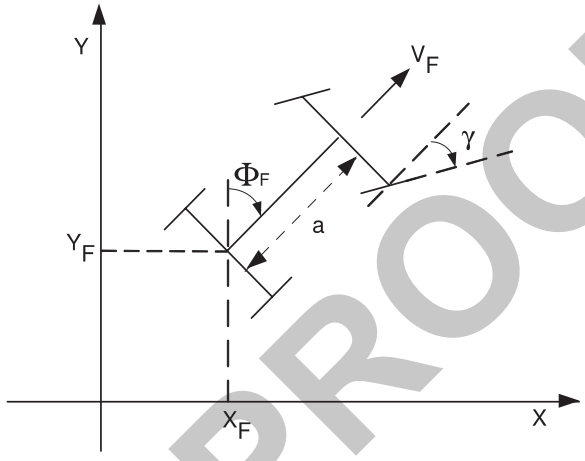

Fig. 3. Pose formulation of the follower vehicle.

A gyroscope is introduced to reduce the problem of orientation drift. A gyroscope can be mounted at the center of the rear axle, the position of which will be the reference point for the localization of the follower vehicle. The gyroscope provides information regarding the change in orientation of the vehicle with a reasonable angular bias. An off the shelf, optical fiber gyroscope[2] achieves an angular bias of less than $1^\circ\,\mathrm{hr}^{-1}$ (Liu et al. 2005).

2. In our project, we use the KVH DSP-5000 Fiber Optic Gyro from KVH Industrial, Inc. www.kvh.com.

Under the Ackerman model, the motion of the follower can now be described in terms of a nonlinear state transition equation as:

$$\begin{aligned}\mathbf{x}_F(k+1) &= \begin{bmatrix} x_F(k+1) \\ y_F(k+1) \\ \phi_F(k+1) \end{bmatrix} \\ &= \begin{bmatrix} x_F(k) + V_F(k)\triangle T \sin\phi_F(k) \\ y_F(k) + V_F(k)\triangle T \cos\phi_F(k) \\ \phi_F(k) + \dfrac{V_F(k)\triangle T}{a}\tan\gamma\,(k) \end{bmatrix} \\ &+ \mathbf{w}_F(k)\end{aligned}$$

where x_F and y_F are the coordinates of the follower with respect to the global coordinate system and ϕ_F is its heading angle. $\mathbf{w}_F(k)$ denotes the process noise vector. The control inputs, $V_F(k)$ and $\gamma\,(k)$ are the longitudinal velocity and steering angle of the vehicle, respectively. $\triangle T$ is the sampling time of the localization process.

As the gyroscope is used to measure the orientation of the vehicle, the observation model is:

$$\varphi_{\text{gyro}}(k) = \begin{bmatrix} 0 & 0 & 1 \end{bmatrix} \begin{bmatrix} x_F(k) \\ y_F(k) \\ \phi_F(k) \end{bmatrix} + \mu_F(k) \qquad (12)$$

PROOF ONLY

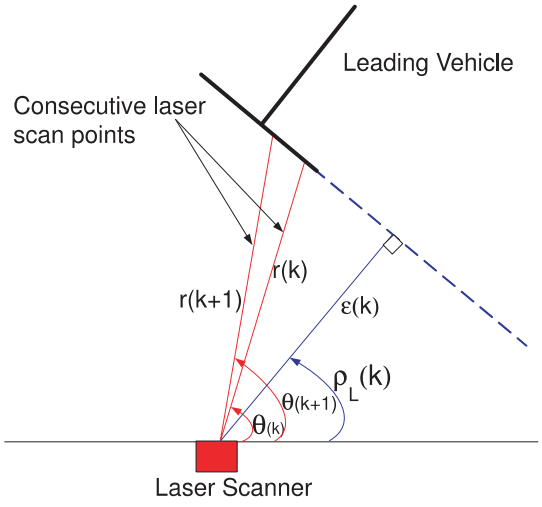

Fig. 4. A line model representation for detection of the leader vehicle. All measurements are made with respect to the laser scanner frame of reference.

where $\mu_{\mathrm{F}}(k)$ denotes the gyro sensor measurement noise. With the above system and measurement models (equation (12)), the updated pose of the follower vehicle can be obtained using filtering techniques such as Extended Kalman or Particle filters (Thrun et al. 2005). This updated information will be used as the observation information to update the pose of the leader vehicle as described in Section 5.2.3.

5.2. Detection and Tracking of the Leader Vehicle

The tracking of the leader vehicle involves its detection and the estimation of its pose with respect to the follower.

5.2.1. Detecting the Target Vehicle

Target vehicle detection is one of the most important tasks for reliable vehicle following. Typical objects on the road are cars, trucks, buses, pedestrians and cyclists, which must not be misclassified. In the current experiments, we used a laser scanner (SICK LMS291) to perceive the environment. As a first approximation, the rear of the leader vehicle is assumed to be represented by a line in the 2D laser range data. Simplistically, at this stage, a line model will be used to detect the leader vehicle.

A data segmentation procedure has to be carried out in order to identify the potential candidates for line modeling. With the segmented data, a line modeling procedure will be performed to estimate the pose of the possible leader. Simple Nearest Neighbor based data association, based on the previous leader pose and its current predicted pose, is then carried out to estimate its updated pose.

As for the line model, the Hough Transform representation is proposed. The shortest distance, $\varepsilon(k)$, from the laser scanner to the target line, and its corresponding bearing, $\rho_{\mathrm{L}}(k)$ are shown in Figure 4. The Hough Transform representation, for line extraction, has been successfully implemented in many robotic applications (Nguyen et al. 2005). However, there are issues that need to be addressed before implementing the algorithm. Firstly, choosing an appropriate grid size in the Hough Space is a problem. Secondly, sensor uncertainties are not considered in the Hough Transform implementation. We therefore propose the use of a recursive filter (in this case the EKF) to address the above issues while maintaining the use of the Hough Transform parameters $\varepsilon(k)$ and $\rho_{\mathrm{L}}(k)$. For a given line, $\varepsilon(k)$ and $\rho_{\mathrm{L}}(k)$ are constant. With this information and the assumption of a straight line, it is possible to predict the next range value $r(k+1)$ in terms of $r(k)$, $\rho_{\mathrm{L}}(k)$ and $\theta(k)$, where $\theta(k)$ denotes the bearing of the point with range $r(k)$ at time k. The prediction equation is:

$$\begin{aligned}\mathbf{X}_{\text{line}}(k+1) &= \begin{bmatrix} r(k+1) \\ \theta(k+1) \\ \rho_{\mathrm{L}}(k+1) \\ \varepsilon(k+1) \end{bmatrix} \\ &= \begin{bmatrix} \dfrac{r(k)\cos(\rho_{\mathrm{L}}(k)-\theta(k))}{\cos(\rho_{\mathrm{L}}(k)-\theta(k)-\Psi)} \\ \theta(k)+\Psi \\ \rho_{\mathrm{L}}(k) \\ \varepsilon(k) \end{bmatrix} \\ &+ \quad \mathbf{w}_l(k) \end{aligned} \tag{13}$$

where $\Psi = 0.5^\circ$ is the angular resolution of the laser scanner used and $\mathbf{w}_l(k)$ is the process noise vector.

Since, in general, a range finder produces range values in a sequence with respect to the scanning angle, an EKF can be formulated to recursively estimate the parameters, $\hat{\rho_{\mathrm{L}}}(k|k)$ and $\hat{\varepsilon}(k|k)$, of the line. The estimated values of $\rho_{\mathrm{L}}(k)$, $\varepsilon(k)$ and the corresponding error covariance matrix,

$$\Sigma_{\text{line model}} = \begin{bmatrix} \sigma^2_{\rho_{\mathrm{L}}} & \sigma_{\rho_{\mathrm{L}}}\sigma_{\varepsilon} \\ \sigma_{\varepsilon}\sigma_{\rho_{\mathrm{L}}} & \sigma^2_{\varepsilon} \end{bmatrix} \tag{14}$$

will be used for estimating the pose of the leader vehicle.

5.2.2. Estimating the Pose of the Target Vehicle

From the line model, we can obtain estimates of the range S to the center point of the rear of the leader vehicle and its bearing θ relative to the sensor by using the geometric properties shown in Figure 5.

PROOF ONLY

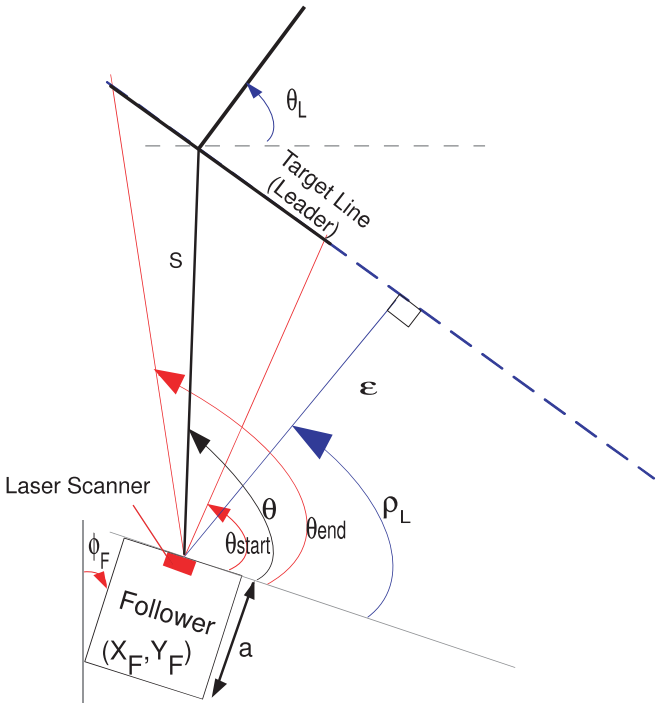

Fig. 5. Estimation of the range S, bearing θ and orientation ρ_L of the leader vehicle.

Taking the center of the rear side of the target vehicle as a reference, the bearing of the target vehicle is simply

$$\theta = \frac{\theta_{\text{start}} + \theta_{\text{end}}}{2}. \tag{15}$$

We assume that the errors in determining θ_{start} and θ_{end} are uncorrelated. As θ_{start} and θ_{end} are measured relative to the sensor frame, the above assumption is valid when conditioned to the pose of the follower. The estimated bearing variance, in vehicle coordinates, may be computed as:

$$\sigma_\theta^2 = \nabla_\Theta \begin{bmatrix} \sigma_{\theta_{\text{start}}}^2 & 0 \\ 0 & \sigma_{\theta_{\text{end}}}^2 \end{bmatrix} \nabla_\Theta{}^T = \frac{1}{2}\sigma_{\text{laser},\theta}^2 \tag{16}$$

where

$$\nabla_\Theta = \begin{bmatrix} \frac{\partial\theta}{\partial\theta_{\text{start}}} & \frac{\partial\theta}{\partial\theta_{\text{end}}} \end{bmatrix} \tag{17}$$

$$\frac{\partial\theta}{\partial\theta_{\text{start}}} = \frac{\partial\theta}{\partial\theta_{\text{end}}} = \frac{1}{2} \tag{18}$$

assuming

$$\sigma_{\theta_{\text{start}}}^2 = \sigma_{\theta_{\text{end}}}^2 = \sigma_{\text{laser},\theta}^2 \tag{19}$$

where $\sigma_{\text{laser},\theta}^2$ is the variance of the angular measurement of the laser scanner.

The estimated range S, computed from the sensor to the center of the target line is:

$$S = \frac{\varepsilon}{2}\left\{\frac{1}{\cos(\rho_L - \theta_{\text{start}})} + \frac{1}{\cos(\rho_L - \theta_{\text{end}})}\right\} \tag{20}$$

and the range variance is:

$$\begin{aligned}\sigma_S^2 &= \begin{bmatrix} \frac{\delta S}{\delta\varepsilon} & \frac{\delta S}{\delta\rho_L} & \frac{\delta S}{\delta\theta_s} & \frac{\delta S}{\delta\theta_e} \end{bmatrix} \\ &\times \begin{bmatrix} \sigma_\varepsilon^2 & 0 & 0 & 0 \\ 0 & \sigma_{\rho_L}^2 & 0 & 0 \\ 0 & 0 & \sigma_{\theta_s}^2 & 0 \\ 0 & 0 & 0 & \sigma_{\theta_e}^2 \end{bmatrix} \begin{bmatrix} \frac{\delta S}{\delta\varepsilon} \\ \frac{\delta S}{\delta\rho_L} \\ \frac{\delta S}{\delta\theta_s} \\ \frac{\delta S}{\delta\theta_e} \end{bmatrix} \\ &= \left(\frac{\delta S}{\delta\varepsilon}\right)^2 \sigma_\varepsilon^2 + \left(\frac{\delta S}{\delta\rho_L}\right)^2 \sigma_{\rho_L}^2 \\ &+ \left(\frac{\delta S}{\delta\theta_s}\right)^2 \sigma_{\theta_s}^2 + \left(\frac{\delta S}{\delta\theta_e}\right)^2 \sigma_{\theta_e}^2 \end{aligned} \tag{21}$$

where θ_s and θ_e denote θ_{start} and θ_{end} respectively,

$$\frac{\delta S}{\delta\varepsilon} = \frac{1}{2}\left[\frac{1}{\cos(\rho_L - \theta_s)} + \frac{1}{\cos(\rho_L - \theta_e)}\right], \tag{22}$$

$$\frac{\delta S}{\delta\rho_L} = \frac{\varepsilon}{2}\left[\frac{\sin(\rho_L - \theta_s)}{\cos^2(\rho_L - \theta_s)} + \frac{\sin(\rho_L - \theta_e)}{\cos^2(\rho_L - \theta_e)}\right], \tag{23}$$

$$\frac{\delta S}{\delta\theta_s} = \frac{-\varepsilon}{2}\left[\frac{\sin(\rho_L - \theta_s)}{\cos^2(\rho_L - \theta_s)}\right], \tag{24}$$

$$\frac{\delta S}{\delta\theta_e} = \frac{-\varepsilon}{2}\left[\frac{\sin(\rho_L - \theta_e)}{\cos^2(\rho_L - \theta_e)}\right], \tag{25}$$

and σ_ε^2 and $\sigma_{\rho_L}^2$ are the variances extracted from the covariance matrix $\Sigma_{\text{line model}}$, as explained in Section 5.2.1 (equation (14)).

5.2.3. Localizing the Leader Vehicle with the Virtual Trailer Link Model

From the laser range finder data, we are able to obtain the range S to the rear center point, its bearing θ and the orientation ρ_L of the leading vehicle with respect to the follower, as described in Sections 5.2.1 and 5.2.2.

In our application, we have set the sampling time for the data acquisition of the laser information to be 0.1 seconds. With this sampling rate, we (reasonably) assume that the leader vehicle is travelling at a constant velocity and a constant turning rate, allowing the use of a constant velocity kinematic model.

PROOF ONLY

The kinematic model for the leader vehicle and the corresponding VT link, as illustrated in Figure 1, is:

$$\mathbf{X}_{\mathrm{L}}(k+1) = \begin{bmatrix} x_{\mathrm{L}}(k+1) \\ y_{\mathrm{L}}(k+1) \\ \theta_{\mathrm{L}}(k+1) \\ \dot{\theta}_{\mathrm{L}}(k+1) \\ V_{\mathrm{L}}(k+1) \\ \phi_{\mathrm{L}}(k+1) \\ \dot{\phi}_{\mathrm{L}}(k+1) \end{bmatrix} \tag{26}$$

$$= \begin{bmatrix} x_{\mathrm{L}}(k) + V_{\mathrm{L}}(k)\Delta T\cos(\theta_{\mathrm{L}}(k)) \\ y_{\mathrm{L}}(k) + V_{\mathrm{L}}(k)\Delta T\sin(\theta_{\mathrm{L}}(k)) \\ \theta_{\mathrm{L}}(k) + \Delta T\dot{\theta}_{\mathrm{L}}(k) \\ \dot{\theta}_{\mathrm{L}}(k) \\ V_{\mathrm{L}}(k) \\ \phi_{\mathrm{L}}(k) + \Delta T\dot{\phi}_{\mathrm{L}}(k) \\ -\dfrac{V_{\mathrm{L}}(k)\sin(\phi_{\mathrm{L}}(k))}{a} + \dot{\theta}_{\mathrm{L}}(k)(1+\cos(\phi_{\mathrm{L}}(k))) \end{bmatrix} + \mathbf{w}_{\mathrm{L}}(k) \tag{27}$$

where $x_{\mathrm{L}}(k+1)$, $y_{\mathrm{L}}(k+1)$, $\theta_{\mathrm{L}}(k+1)$, $\dot{\theta}_{\mathrm{L}}(k+1)$ and $V_{\mathrm{L}}(k+1)$ are the x and y positions, orientation, angular velocity and longitudinal velocity of the leader vehicle, with respect to the given reference coordinate system, respectively. ϕ_{L} is the trailer angle between the axis of the virtual trailer and the longitudinal axis of the leader vehicle, $\dot{\phi}_{\mathrm{L}}$ is the rotational speed of the trailer and $\mathbf{w}_{\mathrm{L}}(k)$ is the process noise vector.

As the model described above is a nonlinear system, we again use the EKF to predict the states of the leader vehicle and the corresponding virtual trailer. Hence the Jacobian of the system model is:

$$\nabla f_{\mathrm{L}}(k) = \begin{bmatrix} 1 & 0 & h & 0 & b & 0 & 0 \\ 0 & 1 & c & 0 & d & 0 & 0 \\ 0 & 0 & 1 & \Delta T & 0 & 0 & 0 \\ 0 & 0 & 0 & 1 & 0 & 0 & 0 \\ 0 & 0 & 0 & 0 & 1 & 0 & 0 \\ 0 & 0 & 0 & 0 & 0 & 1 & \Delta T \\ 0 & 0 & 0 & e & f & g & 0 \end{bmatrix} \tag{28}$$

where

$$\begin{aligned} h &= -V_{\mathrm{L}}(k)\Delta T\sin(\theta_{\mathrm{L}}(k)), \\ b &= \Delta T\cos(\theta_{\mathrm{L}}(k)), \\ c &= V_{\mathrm{L}}(k)\Delta T\cos(\theta_{\mathrm{L}}(k)), \\ d &= \Delta T\sin(\theta_{\mathrm{L}}(k)), \\ e &= 1+\cos(\phi_{\mathrm{L}}(k)), \\ f &= [-\sin(\phi_{\mathrm{L}}(k))]/a \text{ and} \\ g &= -[V_{\mathrm{L}}(k)\cos(\phi_{\mathrm{L}}(k))]/a - \dot{\theta}_{\mathrm{L}}(k)\sin(\phi_{\mathrm{L}}(k)). \end{aligned}$$

With the laser scanner mounted on the follower vehicle, we are able to estimate the pose of the leader vehicle as outlined in Section 5.2.1 and 5.2.2. An 'indirect' measurement formulation is used so that the measurement vector used for computing the pose of the leader vehicle, from Figure 5, is:

$$\mathbf{Z}_{\mathrm{L}}(k) = \begin{bmatrix} Z_{x_{\mathrm{L}}} \\ Z_{y_{\mathrm{L}}} \\ Z_{\theta_{\mathrm{L}}} \end{bmatrix}$$

$$= \begin{bmatrix} x_{\mathrm{F}} + S\cos(\theta-\phi_{\mathrm{F}}) + a\cos\left(\dfrac{\pi}{2}-\phi_{\mathrm{F}}\right) \\ y_{\mathrm{F}} + S\sin(\theta-\phi_{\mathrm{F}}) + a\sin\left(\dfrac{\pi}{2}-\phi_{\mathrm{F}}\right) \\ \rho_{\mathrm{L}} - \phi_{\mathrm{F}} \end{bmatrix} + \boldsymbol{\mu}_{\mathrm{L}}(k) \tag{29}$$

with the observation covariance matrix:

$$\Sigma Z_{\mathrm{L}}(k+1) = \nabla\mathbf{Z}_{\mathrm{L}}\mathbf{R}_{\mathbf{Z}_{\mathrm{L}}}\nabla\mathbf{Z}_{\mathrm{L}}^{T} \tag{30}$$

where $\boldsymbol{\mu}_{\mathrm{L}}(k)$ is the measurement noise vector and the Jacobian of the measurement model is

$$\nabla\mathbf{Z}_{\mathrm{L}} = \begin{bmatrix} \frac{\partial\mathbf{Z}_{\mathrm{L}}(k)}{\partial S} & \frac{\partial\mathbf{Z}_{\mathrm{L}}(k)}{\partial\theta} & \frac{\partial\mathbf{Z}_{\mathrm{L}}(k)}{\partial\rho_{\mathrm{L}}} & \frac{\partial\mathbf{Z}_{\mathrm{L}}(k)}{\partial x_{\mathrm{F}}} & \frac{\partial\mathbf{Z}_{\mathrm{L}}(k)}{\partial y_{\mathrm{F}}} & \frac{\partial\mathbf{Z}_{\mathrm{L}}(k)}{\partial\phi_{\mathrm{F}}} \end{bmatrix}. \tag{31}$$

The 6×6 measurement noise covariance matrix, assuming the laser data to be independent (refer to the following section for an explanation of this assumption) of the pose of the follower vehicle, is

$$\mathbf{R}_{Z_{\mathrm{L}}} = \begin{bmatrix} \sigma^2_{SS} & \sigma^2_{\theta S} & \sigma^2_{\rho_{\mathrm{L}}S} & 0 & 0 & 0 \\ \sigma^2_{S\theta} & \sigma^2_{\theta\theta} & \sigma^2_{\rho_{\mathrm{L}}\theta} & 0 & 0 & 0 \\ \sigma^2_{S\rho_{\mathrm{L}}} & \sigma^2_{\theta\rho_{\mathrm{L}}} & \sigma^2_{\rho_{\mathrm{L}}\rho_{\mathrm{L}}} & 0 & 0 & 0 \\ 0 & 0 & 0 & \sigma^2_{X_{\mathrm{F}}X_{\mathrm{F}}} & \sigma^2_{Y_{\mathrm{F}}X_{\mathrm{F}}} & \sigma^2_{\phi_{\mathrm{F}}X_{\mathrm{F}}} \\ 0 & 0 & 0 & \sigma^2_{X_{\mathrm{F}}Y_{\mathrm{F}}} & \sigma^2_{Y_{\mathrm{F}}X_{\mathrm{F}}} & \sigma^2_{\phi_{\mathrm{F}}Y_{\mathrm{F}}} \\ 0 & 0 & 0 & \sigma^2_{X_{\mathrm{F}}\phi_{\mathrm{F}}} & \sigma^2_{Y_{\mathrm{F}}\phi_{\mathrm{F}}} & \sigma^2_{\phi_{\mathrm{F}}\phi_{\mathrm{F}}} \end{bmatrix}. \tag{32}$$

PROOF ONLY

5.2.4. A Note on Independence Assumptions

In the problem formulation section, we argued that the vehicle following system can be factored into two separate estimation processes, one for the localization of the follower while the other is used to track the leader vehicle. In our implementation, we have intentionally performed the localization of the follower vehicle first, followed by the tracking of the leader vehicle. By doing so, we can assume that the laser data is *conditionally* independent of the pose of the follower vehicle as we already have the information on the pose of the follower vehicle before estimating the pose of the leader vehicle.

6. System Evaluation

Based on the proposed Bayesian formulation and the system and measurement models for the vehicle following system, we will now provide a case study using the Extended Kalman Filter (EKF) (Bar-Shalom and Fortmann 1998) as the main estimator. Other filters such as the Unscented Kalman Filter or Particle Filter (Thrun et al. 2005) could also be used.

Prior to the analysis of the performance, it is necessary to have a full understanding of the system. The case study of the proposed system uses two different sensors, a gyroscope (Liu et al. 2005) and a laser range scanner together with an EKF, as a way to observe the states of both the leader and follower vehicles. For a successful implementation, three major issues have to be addressed:

- how to associate the current sensor information to the sensor information received in the previous observation (data association problem);
- how to deal with sensor data that is corrupted by the pitching effect of the vehicle; and
- how to impose kinematic constraints on the leader vehicle model.

6.1. Data Association Issues

The information received from the laser scanner reflects the relative pose of the leader vehicle with respect to the follower vehicle. The information received at every time instant does not have a common reference frame as the scanner is in motion together with the follower vehicle. At this early stage in our system, the generally difficult data association problem is assumed to be solved by implementing the nearest neighbor method (Bar-Shalom and Fortmann 1998). A coordinate transformation of the poses of the leader vehicle to a common reference frame, in the previous and current time instances, can be performed. Once the correspondence has been established, we can use the EKF to predict the next pose of the leader vehicle based on the last estimate of the pose and motion of the leader vehicle.

6.2. Measurement Noises and Filter Tuning

As proposed in Section 5.2.3, the computation of the pose of the leader vehicle is indirect. That is, an EKF has been used to estimate the pose of the leader vehicle by considering the center of the rear of the leader vehicle as the measurement, rather than directly using the information from the laser data. Furthermore, the data received from the scanner may be corrupted due to various reasons such as the pitching of the sensor due to the unevenness of the road surface.

The effectiveness of the EKF depends on the accuracy of the observation noise covariance matrix. A static, predetermined covariance matrix in many cases cannot achieve a good estimate of the state of the system. The computed orientation of the leader vehicle can vary significantly if the laser data received is corrupted by the motion of the vehicle that carries the sensor. In our case, if there are outliers in the laser data, the error in estimating the relative position of the leader position will be small compared with the error in estimating the orientation of the leader vehicle. The rapid change in the quality of this orientation data will result in an inaccurate computation of the filter gain and hence in an undesirable, large correction of the estimate of the vehicle's orientation.

In our system, we have proposed a simple and yet effective dynamic observation noise model to improve the effectiveness of the filtering process. In this model, we examine the measurement innovation against the predicted orientation of the leader vehicle. If the innovation is beyond a threshold level, a larger observation noise covariance is used in the filter. The basic concept behind this method is that, if the innovation is large, which implies that there is a large discrepancy between the predicted and measured values, we would rather trust the prediction model than the measurement model, based on our 'unmodeled' knowledge of the negative effect of the sensing, caused by vehicle pitching.

For the fine tuning of the threshold of the aforementioned innovation, various considerations have to be applied. The laser may scan the rear and/or the side surface of the leader vehicle. Both of these surfaces appear as a line and therefore the vehicle's side could be mistaken for the rear of the leader vehicle. With a short sampling interval for the measurement, typically 0.1 seconds to acquire an entire scan in our case, we are certain that any road vehicle will not be able to turn through 90° in this period. We therefore set the threshold level on the orientation innovation to be within $\pm 10^\circ$, to be conservative.

6.3. Kinematic Constraints

Considering that the update rate of our filters is set at 0.1 seconds, the kinematic constraints of the leader vehicle system model, shown in equation (27), are used. We also have knowledge of the maximum speed of the leader vehicle if we know its specifications. In this case, we have set the maximum speed

PROOF ONLY

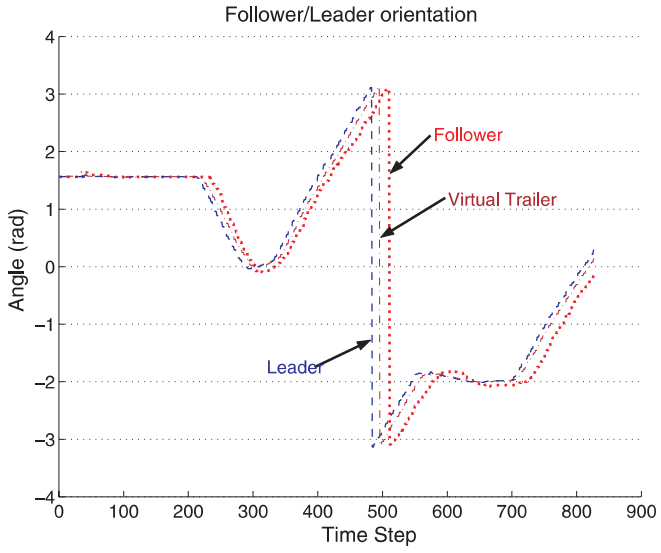

Fig. 6. Orientations of the leader, virtual trailer and follower. (See text for the descriptions of the maneuvers of the vehicles and the virtual trailer.)

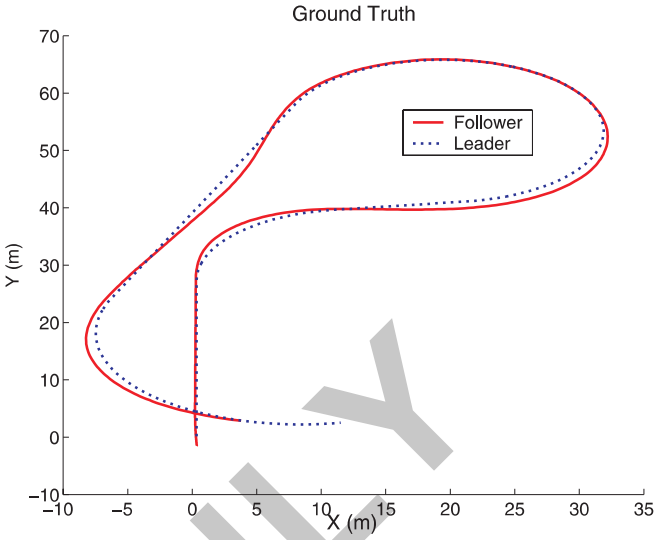

Fig. 7. Ground truth for the leader and follower vehicles.

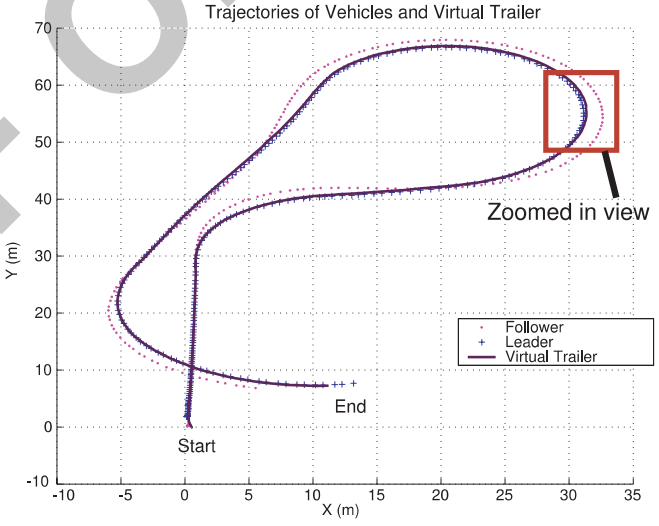

Fig. 8. Simulation run. Various types of paths such as straight line, turning left and right are included. The positions of the virtual trailer follow the path of the leader vehicle closely.

of the leader vehicle to be 3 m s^{-1}. Further, we know that under normal driving conditions on the road, a vehicle cannot be steered beyond a certain angle. Based on these assumptions, we can set constraints on the estimated pose of the leader vehicle. As mentioned in the previous section, measurement noise from the sensor is inevitable. Incorrect estimates of the inter-vehicle spacing result in the incorrect estimate of the velocity of the leader vehicle. Hence, by setting a maximum value for the estimated velocity of the leader, the data association performance can be improved.

7. Experimental Results

To validate the performance of the proposed formulation, simulated and real experiments have been carried out. For demonstration purposes, EKFs will be used as the main estimators in both experiments. Repetitive simulation runs were performed. Figures 6 to 13 show the results of a representative simulation run. Comparisons of the results with those reported from other systems will be made in the real experimental section.

7.1. Simulation Results

Stand-alone software was written to control the leader vehicle. To test the robustness of our formulation, the leader vehicle was commanded to travel first in a straight path (from time 0 to 200, i.e. 0 to 20 s since $\Delta T = 0.1$ s), followed by a clothoid with transition to the right (from time 200 to 300), a tight left turn (large curvature simulating a U-turn path, from time 300 to 500), straight (from time 550 to 700) and finally a clothoid with transition to the left (from time 700 to 820) as shown in Figures 6 and 8. The leader vehicle was commanded to gradually transit from the straight path to the circular path, thus simulating a clothoid path in a typical urban road. During the motion, the leader vehicle was accelerated to various speeds as shown in Figure 11.

Another software system, implementing the proposed formulation, was used to command the follower vehicle. A simple

PROOF ONLY

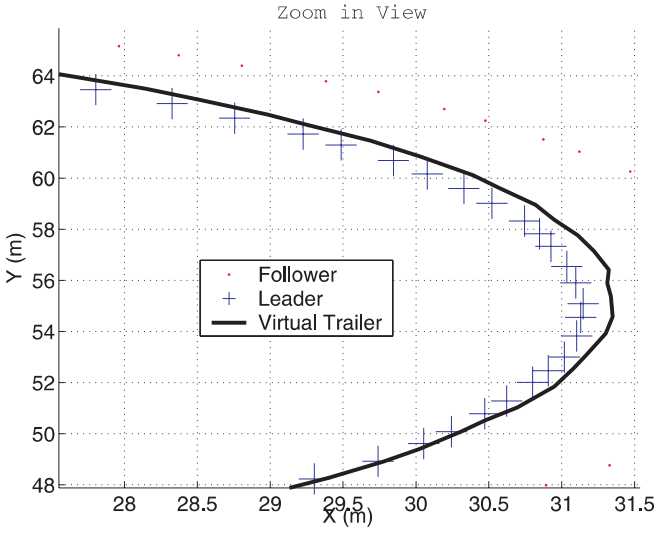

Fig. 9. Zoomed view of Figure 8. The maximum error between the trajectories of the leader and the virtual trailer is approximately 20 cm.

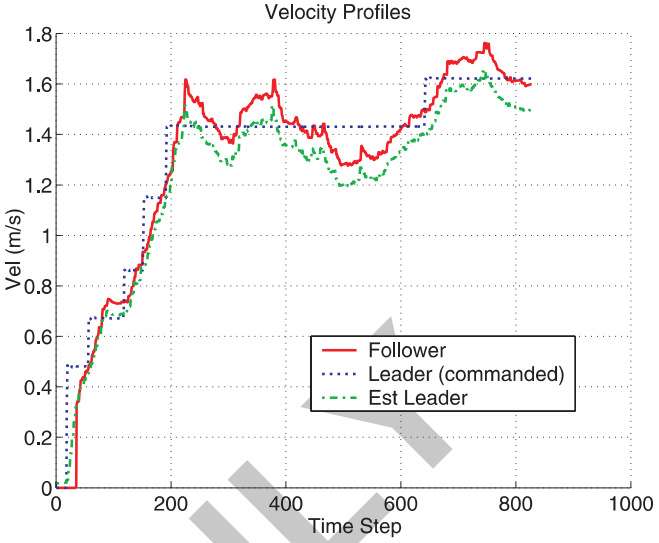

Fig. 11. Commanded and estimated velocity profiles of the leader and follower vehicles.

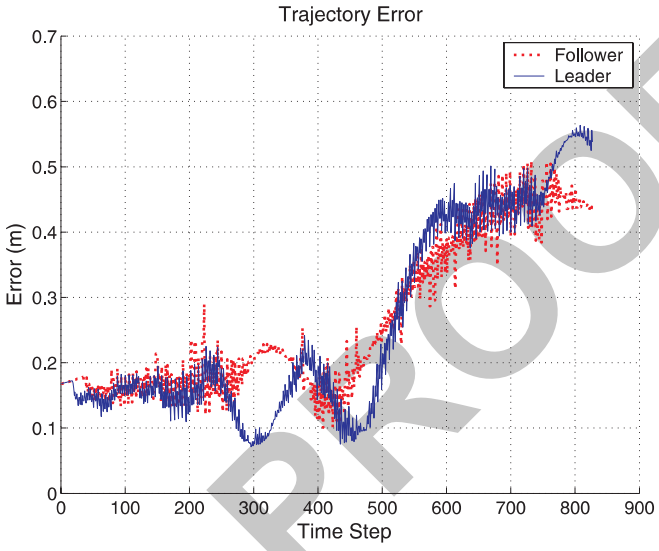

Fig. 10. Positional errors between the ground truth and the estimated positions of the leader and follower vehicles.

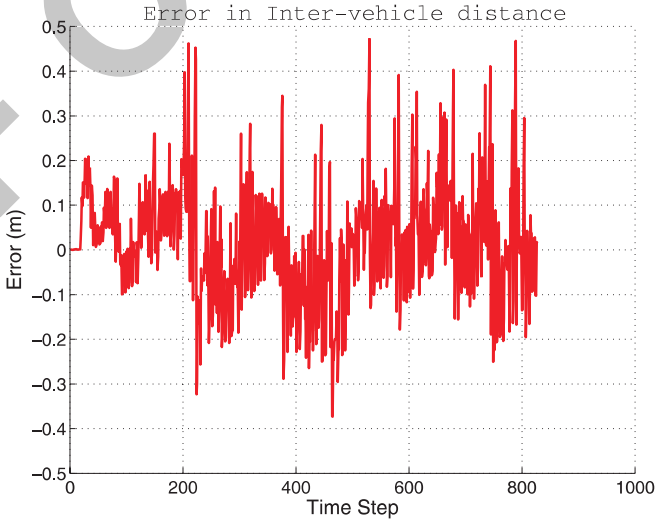

Fig. 12. Inter-vehicle separation errors. The errors were obtained by comparing the difference between the simulated (ground truth) and the estimated inter-vehicle separation.

PROOF ONLY

pure pursuit control strategy was implemented to command the follower vehicle to trail the computed pose of the virtual trailer. To make the simulation results comparable to the actual system, the standard deviation settings of all the sensors used were set as close to the real values as possible. The standard deviations (as obtained from the respective data sheets) of the gyroscope, laser range and laser bearing measurements were set to 1.28°, 5 cm and 0.5°, respectively. The relative pose of the leader vehicle and the virtual trailer, with respect to the follower, were generated at each time step (0.1 s in this case). In this simulation, we assumed that the data association problem, in identifying the leader vehicle, is resolved. Furthermore, the lengths (distance between the front and rear wheels) of both vehicles were 1.2 m (which is identical to the length of our experimental vehicle). Hence, based on the system design requirements for the virtual trailer (Ng et al. 2005), its length was 1.2 m.

From Figure 6, it can be seen that the follower vehicle was able to align itself with the leader vehicle with a small delay.

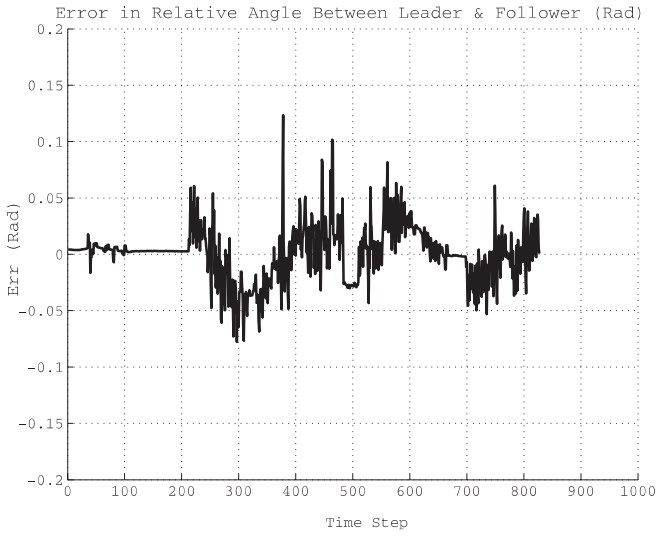

Fig. 13. Relative orientation (between the leader and follower) errors. The errors were obtained by comparing the difference between the real (ground truth) and the estimated relative orientation.

In particular, at time 200 where the leader vehicle has started to make a transition to the right, the follower vehicle has maintained in its straight maneuver despite a change of maneuver from the leader. Similarly, at time 550, the follower vehicle has again maintained its straight maneuver. This is due to the virtual trailer model as described in Section 2. These results are significant in the vehicle following function. With the virtual trailer model, the follower vehicle can trail the trajectory of the leader vehicle and thus avoid hitting the road curb while the vehicles are on a transition path.

From Figure 8, the follower vehicle was able to trail behind the leader vehicle during most of the trajectory. However, there were path deviations between the two vehicles when they negotiate curves. Nevertheless, the estimated poses of the leader vehicle and the virtual trailer were close to each other. A zoomed view of Figure 8 (shown in Figure 9), shows that the maximum path error between the path of the leader vehicle and that of the virtual trailer is less than 20 cm, which occurs when both vehicles make a U-turn. The result is encouraging. Table 1 shows a summary of the error distribution of the path deviation between the leader and virtual trailer. To our knowledge, no other vehicle following system has demonstrated the capability of following a leader in a tight U-turn maneuver (the steering angle of the leader vehicle was set at 20° throughout the turn). Further, the path errors were typically less than 5 cm in all cases. Furthermore, the path deviations between the two vehicles were small (< 30 cm on average) even when the leader vehicle accelerated during turning at times 200 and 650. This error is much smaller than those of the system by Lu and Tomizuka (2005), which reported a maximum path deviation

Table 1. Error distribution for path deviation between leader and virtual trailer.

Error(m)	Frequency
0–0.05	600
0.05–0.10	105
0.10–0.15	100
0.15–0.20	10
> 0.20	5

of 35 cm. A more comprehensive comparison will be made in the real experimental section.

Figure 10 shows a plot of the errors between the actual and estimated positions of the leader and follower vehicles respectively. The positional errors are less than 20 cm from time 0 to 450. As the leader vehicle started to make a tight turn, the positional errors for both vehicles increased with time. The increase in positional errors is expected as only odometry information is used for the localization of both vehicles. Although the absolute positional errors are large (about 50 cm), the relative positional errors between the two vehicles are small as shown in Figure 7. The effect of the absolute positional errors on the vehicle following function is insignificant as the vehicle following function operates on the relative poses of the two vehicles.

Figure 11 shows profiles of the commanded and estimated velocities for the leader vehicle and the commanded velocity of the follower vehicle versus time. The estimated velocity of the leader vehicle was close to its actual velocity versus time. The errors in the estimate are less than $0.2\,\mathrm{m\,s^{-1}}$. From time 0 to 200, when the leader vehicle is moving on a straight path, the estimator has accurately predicted the velocity of the leader vehicle. However, from time 200 to 600, the leader vehicle has been commanded to make various turns. The estimator was unable to predict the velocity of the leader vehicle correctly. As shown in equation (26), the leader vehicle is modeled to be moving at a constant velocity and at a constant turning rate. This model is inadequate for this type of maneuver. This is the main factor in the inaccurate estimation of the leader's velocity. Other available vehicle motion models, such as the Interactive Multiple Model (IMM) filter (Bar-Shalom and Li 2001), could be used to cater for various other types of maneuver.

Figure 12 shows a plot of the errors in the inter-vehicle distance between the two vehicles. The errors were computed by comparing the measured with the actual inter-vehicle distances; 95% and 90% of the errors were within ± 25 cm and ± 20 cm, respectively.

Figure 13 shows a plot of the errors in the relative angle between the two vehicles. The errors were computed by comparing the measured relative angle against the actual relative angle. From time 0 to 200 and 650 to 700, the errors in relative angle were almost zero as expected, since both vehicles

PROOF ONLY

Table 2. Performance of system on roundabout.

Radius(m)	Error (m)
10	< 0.25
20	< 0.18
30	< 0.18
40	< 0.18

Table 3. Performance of system on clothoid.

Straight path to radius, R_c (m)	Error (m)
10	< 0.30
20	< 0.25
30	< 0.18
40	< 0.10

are moving on a straight path. As expected, the errors increase when the vehicles are negotiating turns. As the positional errors for the follower are relatively small, as shown in Figure 8, we are confident that with the proposed formulation the follower vehicle will be able to trail the leader vehicle successfully.

Tables 2 and 3 summarize the performance of the proposed system under a simulated roundabout (circular) and transition paths. The radii of a roundabout can range from 10 m to 40 m. For analysis purposes, both vehicles are commanded to move on the circular path, with various radii. Average path deviations are then computed. The average path deviation between both vehicles are small, in the range of 0.18 m to 0.25 m (Table 2).

As for the transition paths (clothoids), both vehicles are commanded to move on a straight path and gradually steer into the roundabout. The average path deviation between both vehicles is small, in the range of 0.10 m to 0.30 m (Table 3).

7.2. Real Experimental Results

The follower vehicle used in this project is a RobuCar from RoboSoft (http://www.robosoft.fr/robucar.html), as shown in Figure 14. It is a four wheel driven vehicle for outdoor applications. For our experiment, the RobuCar was configured as a rear wheel driving and front wheel steering vehicle. A SICK laser scanner was mounted at the front of the RobuCar. The gyroscope was mounted at the middle of the rear wheel axle. On-board data acquisition cards were installed to capture the laser information, gyroscope readings and wheel encoder speeds. The leader vehicle is a golf cart, Club Car – CarryAll II (http://www.clubcar.com). The leader vehicle was manually driven around the test track which comprised a straight path and clothoids with both left and right transitions. The control issues of the follower vehicle are not considered here. This is

Fig. 14. The leader and follower vehicles. The leader vehicle (Club Car – CarryAll II) is manually driven around the test track in the car park. The follower vehicle is teleoperated to follow the leader. The laser scanner is mounted at the front and the gyroscope is mounted at the center of the rear axle of the follower.

because the main purpose of the experiment is to evaluate the capability of the proposed formulation in tracking the leader vehicle using the virtual trailer while the follower vehicle is in motion. Hence, the follower vehicle was manually driven to trail behind the leader vehicle.

The test track was located in a carpark on campus. As there are tall buildings in the vicinity, the GPS system failed to function satisfactorily. Hence, we designed the experiment so that approximate ground truth trajectories for both vehicles were easily obtained for comparison purposes.

Figure 15 shows the plot of the paths for the follower, leader and virtual trailer. The path of the virtual trailer follows the path of the leader vehicle. Moreover, the path deviations between the estimated leader vehicle and the virtual trailer are small (typically < 5 cm) when the vehicles are moving along a straight path. However, there are errors of about 15 cm when the vehicles are negotiating the curve, at positions near $(25, 8)$ in Figure 15 and at time 500 as shown in Figure 16. By investigating the raw laser data, it was observed that the main cause of these deviations was from corrupted range data. Also, it was observed that the data was corrupted at time 700 as shown in Figure 16. Due to the pitching of the follower vehicle, the laser points were corrupted as shown in Figure 17. The segmentation and line extraction algorithms were unable to correctly identify the leader vehicle thus causing the false estimation of the pose of the leader vehicle. Since measurement data is then lost, the filter has to rely on the predictions. This has contributed to the path deviations. Once the measurement data was restored, the filter functioned as expected and

PROOF ONLY

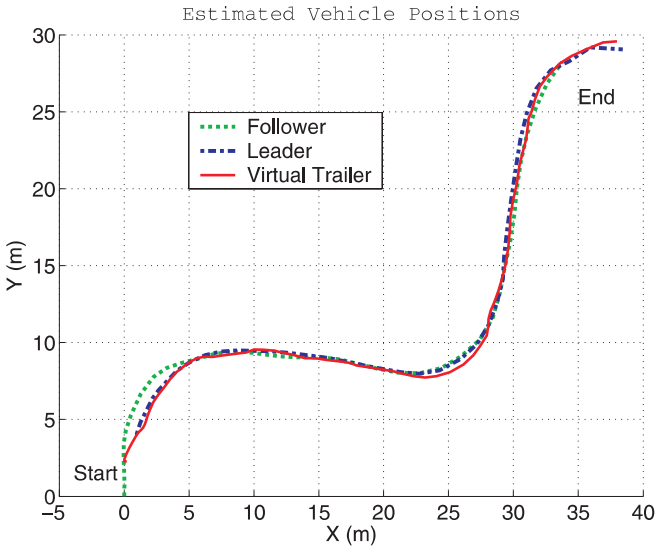

Fig. 15. The estimated vehicle and virtual trailer trajectories. Both the leader and follower vehicles were driven manually on a test track. The estimated trajectories for both the leader vehicle and the virtual trailer are similar.

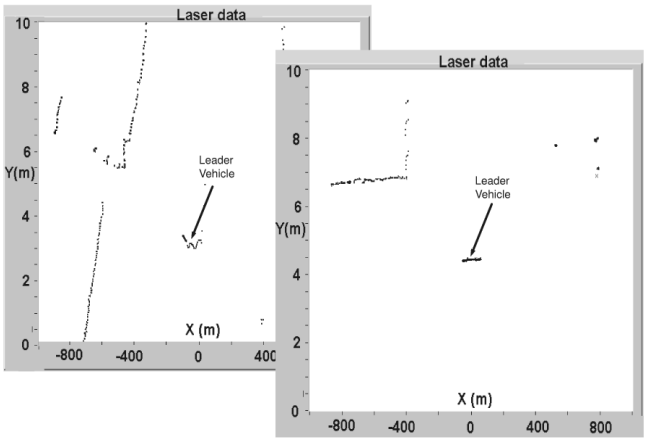

Fig. 17. Projection of the range data from the laser scanner onto the $X - Y$ plane. The figure on the right shows good laser returns, reflected from the leader vehicle. The laser data can be easily fitted to a straight line model. However, the laser data presented in the left figure causes the straight line model to give a false detection.

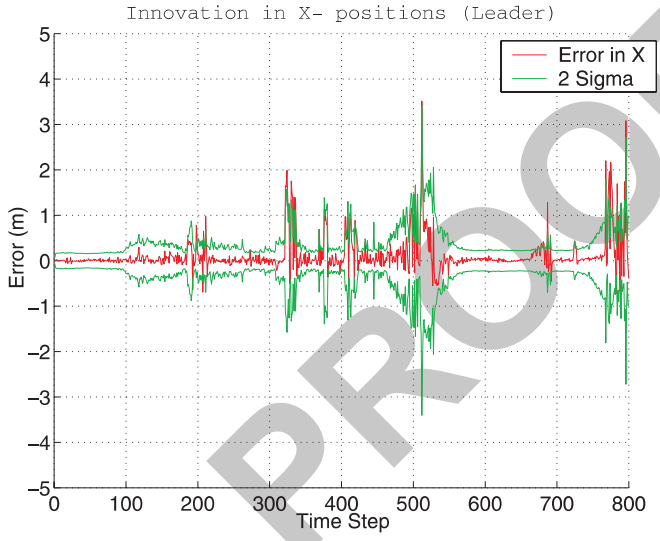

Fig. 16. Residues in the x position and the 2-sigma upper and lower bounds. The residues are well within the bounds. The residues are noisy at approximately time 500. This is due to the noisy data from the laser sensor.

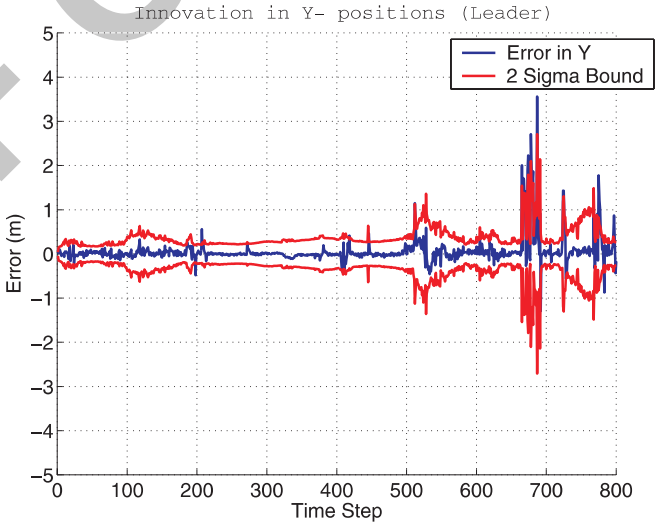

Fig. 18. Residues in the y position of the leader and the 2-sigma upper and lower bounds. The residues are well within the bounds.

PROOF ONLY

the errors in the poses of the leader and virtual trailer were reduced significantly.

Figures 16 to 19 show the pose innovations of the leader vehicle. It is interesting to observe from Figures 16 and 18 that the positional errors of the leader vehicle fall well within its estimated 2σ bounds. The majority of the 2σ bounds for both the x and y position estimates are less than 20 cm. The positional errors become larger when the leader vehicle turns. As described in the previous paragraph, the larger errors were due to the corrupted observation data. Regarding the orientation innovation for the leader, the errors were small as shown in Figure 19.

A direct comparison of the performance of our system with previous work is not straightforward as the variables used to describe vehicle's poses are not always the same from one system to another. However, to give an indication of the achieved

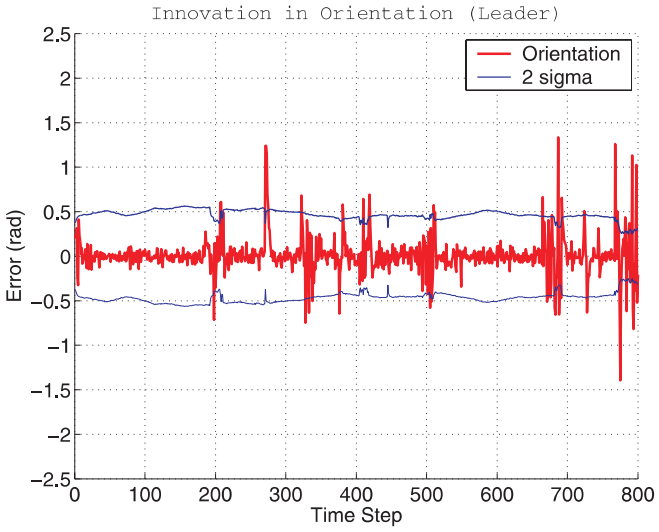

Fig. 19. Residues in the orientation of the leader vehicle and the 2-sigma upper and lower bounds. The residues are well within the bounds.

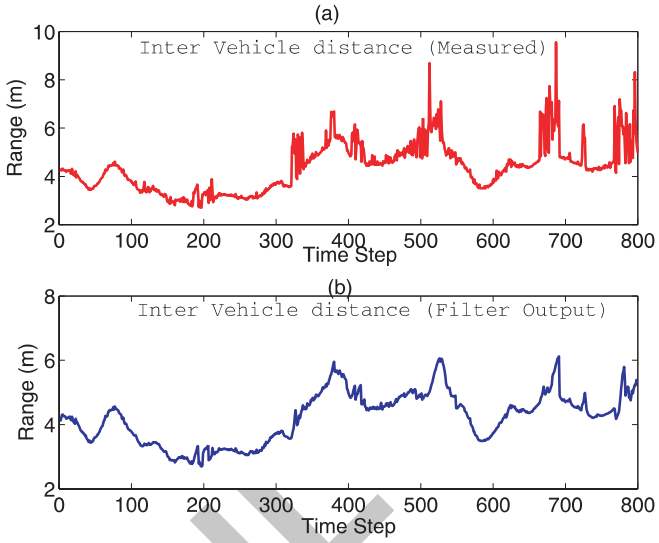

Fig. 20. Inter-vehicle distance between the leader and follower vehicles. The top figure shows the inter-vehicle distance computed from the raw laser data. The lower figure shows the filtered inter-vehicle distance.

performance, a comparison of the maximum path deviation[3] with the experiments carried out by Stefan (2000), Wang and Xu (2000) and Lu and Tomizuka (2005) is given. The path-based vehicle following algorithm implemented by Stefan (2000) achieved an average path deviation of 20 cm with maximum path deviation (between the two vehicles) of approximately 70 cm. The system implemented by Lu and Tomizuka (2005) achieved an average path deviation of 15 cm and a maximum path deviation of 35 cm. The vehicle following system by Wang and Xu (2000) has achieved an average path deviation of 30 cm and a maximum path deviation of 50 cm. As for our case, the maximum path deviation between the leader vehicle and the virtual trailer is 15 cm. The comparison is only an indication as we have not yet implemented the controller for the follower vehicle. However, at this stage our system is already performing at least 2 times better with respect to the maximum path deviation than the other systems. Furthermore, in view of the controller designed for vehicle following by Lu and Tomizuka (2005), typical path deviation errors are of the order of magnitude of 5 cm to 30 cm. We are confident that with a similar vehicle controller, our system can perform similarly to the system proposed by Lu and Tomizuka (2005) without the use of road markers.

An advantage of the suggested filter formulation is shown in Figure 20. This figure compares the inter-vehicle distances (S in Figure 5), computed from the raw laser range data (Figure 20a) and the estimated value (equation (20)) (Figure 20b). Due to the pitching effect of both vehicles, Figure 20a shows many inter-vehicle spurious values (which in reality would be impossible as the inter-vehicle distance cannot change instantaneously). Figure 20b shows the estimated value which gives a more feasible result, as the changes in the distances are realistic. If the data in Figure 20a were fed into a vehicle following controller, an undesirable response would result as the follower vehicle will be commanded to accelerate at one instant and decelerate at the next.

3. For other similar work, it is the deviation between the two vehicles, and for our case, it is the deviations between the leader vehicle and the virtual trailer as we have not yet implemented a fully automated vehicle following system

8. Conclusions and Future Work

We have demonstrated a Bayesian formulation, together with a virtual trailer link model, aimed at producing a safe autonomous vehicle following system. With this formulation, and the dynamic modelling of the uncertainty in the sensor information, the potential for an autonomous vehicle following function has been demonstrated.

We have shown that a vehicle following system may be formulated as a factored joint posterior Bayesian estimation process. This formulation allows the separate estimation of the poses of the follower and leader vehicles. The pose of the follower vehicle can be predicted by using on-board odometry and a gyroscope. The pose of the leader can be estimated with a Bayesian filter by using the information from a laser scanner, which is mounted on the follower vehicle, together with the estimated pose of the follower vehicle. This is based on the justifiable assumption that the laser measurements and the odometry data are independent when conditioned on the pose of the follower vehicle. This assumption leads to a factored vehicle following system where we can perform the localization

PROOF ONLY

of the follower vehicle prior to the estimation of the pose of the leader vehicle. To estimate the pose of the leader vehicle, the measurement uncertainties in the sensor data have to be compensated for. As both the leader and follower vehicles are constantly in motion, the data from the laser scanner can be corrupted.

As the true values of the states of both vehicles are unknown, we have used the innovation sequences as a method of analyzing the performance of our formulation. Our experimental results have provided evidence that it is feasible to use a factored solution to the vehicle following system with two separate Bayesian estimation filters. The innovation sequences for both the position and orientation of the leader vehicle are well within the 2σ confidence bounds. Furthermore, in the experiments shown, the maximum path deviation resulting from our system is two times smaller than the control errors of similar systems in the literature.

To make the estimation of the poses of both vehicles more robust, it would be interesting to incorporate the range information of the external features, such as lamp posts and trees on the road, into the estimation formulation. Future work on deploying Simultaneous Localization and Map Building (SLAM) (Dissanayake et al. 2001) for vehicle following will be studied.

Acknowledgements

We would like to thank John Mullane and Tan Chai Soon of NTU for setting up the RobuCar for our experiments. Part of this work was funded by the second author's A*STAR-SERC project 042-101-0017 entitled 'Collaborative Autonomous Systems for Built Environments(CARSyB)', Singapore.

References

Bar-Shalom, Y. and Fortmann, T. E. (1998). *Tracking and Data Association*. Mathematics in Science and Engineering. Academic Press.

Bar-Shalom, Y. and Li, X. R. (2001). *Estimation with Application to Tracking and Navigation*. John Wiley and Sons Inc.

Borodani, P. (2000). Full automatic control for trucks in a towbar system. In *Proceedings of International Symposium on Advanced Vehicle Control*, pp. 131–138.

Chen, C., Wang, H., and Ng, T. C. (2004). Target tracking and path planning for vehicle following in jungle environment. In *8th International Conference on Control, Automation, Robotics and Vision*, pp. 455–460.

Committee on Army UGV Technology (2002). *Technology Development for Army Unmanned Ground Vehicles*. Washington, D.C.: The National Academies Press.

Dissanayake, G., Newman, P., Clark, S., Durrant-Whyte, H. F., and Csobra, M. (2001). A solution to simultaneous localisation and map building (SLAM) problem. *IEEE Transactions of Robot Automation,* **17**(3): 229–241.

Fujioka, T. and Suzuki, K. (1994). Lateral autonomous driving by sliding control. In *Proceedings of International Symposium on Advanced Vehicle Control*, pp. 432–437.

Liu, B., Adams, M. D., and Guzmàn, J. I. (2005). Multi-aided inertial navigation for ground vehicles in outdoor uneven environments. In *IEEE International Conference on Robotics & Automation (ICRA)*, pp. 4703–4708.

Lu, G. and Tomizuka, M. (2005). Vehicle following as backup control schemes for magnet-magnetometer-based automated highways. *IEEE Transactions on Control System and Technology,* **3**(2): 274–285.

National Academy of Engineering (1998). Frontiers of engineering: Report on leading edge engineering from 1997. In *Symposium on Frontiers of Engineering*, pp. 89–102.

Ng, T. C., Adams, M. D., and Guzmàn, J. I. (2005). Autonomous vehicle-following systems: A virtual trailer link model. In *Proceedings of International Conference on Intelligent Robots and Systems (IROS)*, pp. 2968–2973.

Ng, T. C., Guzmàn, J. I., Shen, J., Gong, Z., and Chen, C. (2004). Vehicle following with obstacle avoidance capabilities in natural environments. In *Proceedings of IEEE International Conference on Robotics and Automation*, pp. 4283–4288.

Nguyen, V., Martinelli, A., Tomatis, N., and Siegwart, R. (2005). A comparison of line extraction algorithms using 2d laser rangerfinder for indoor mobile robotics. In *IEEE International Robotics and System, IROS*, pp. 1829–1834.

Parent, M. (2004). Automated urban vehicles: State of the art and future directions. In *Proceedings of 8th International Conference on Control, Automation, Robotics and Vision*, pp. 138–142.

Sheikholeslam, S. and Desoer, C. (1991). Longitudinal control of a platoon of vehicles with no communication of the lead vehicle information. In *Proceedings of American Control Conference*, Volume 3, pp. 3102–3106.

Stefan, K. (2000). *Design, Simulation and Implementation of a Vision-Based Vehicle-Following System*. Ph. D. thesis, Bereich 12/13 Fakultat fur Mathematik und Physik, Universität Tüubingen.

Swaroop, D. and Hedrick, J. K. (1996). String stability of interconnected systems. In *IEEE Transactions on Automation and Control*, Volume 41(3), pp. 349–356.

Swaroop, D. and Yoon, S. (1999). The design of a controller for a following vehicle in an emergency lane change maneuver. Technical Report 20 Working paper: UCB-ITS-PWP-99-3, California Partners for Advanced Transit and Highway (PATH).

Thrun, S., Burgard, W., and Fox, D. (2005). *Probabilistic Robotics*. The MIT Press.

Wang, D. W. and Xu, G. (2000). Tracking stability analysis of nonholonomic wheeled mobile robots. In *Proceedings of the American Control Conference*, pp. 3274–3278.

PROOF ONLY